Photocatalytic H_2 Evolution under Visible-Light Irradiation over Band-Structure-Controlled $(CuIn)_xZn_{2(1-x)}S_2$ Solid Solutions

Issei Tsuji,[†] Hideki Kato,[†] Hisayoshi Kobayashi,[‡] and Akihiko Kudo*[,†,§]

Department of Applied Chemistry, Faculty of Science, Tokyo University of Science, 1-3 Kagurazaka, Shinjuku-ku, Tokyo 162-8601, Japan, Department of Chemistry and Bioscience, Faculty of Chemical Technology, Kurashiki University of Science and the Arts, 2640 Nishinoura, Tsurajima, Kurashiki 712-8505, Japan, and Core Research for Evolutional Science and Technology, Japan Science and Technology Agency, Japan

Received: November 19, 2004; In Final Form: February 1, 2005

$(CuIn)_xZn_{2(1-x)}S_2$ solid solutions between a ZnS photocatalyst with a wide band gap and $CuInS_2$ with a narrow band gap showed photocatalytic activities for H_2 evolution from aqueous solutions containing sacrificial reagents SO_3^{2-} and S^{2-} under visible-light irradiation ($\lambda \geq 420$ nm). Pt (0.5 wt %)-loaded $(CuIn)_{0.09}Zn_{1.82}S_2$ with a 2.3-eV band gap showed the highest activity for H_2 evolution, and the apparent quantum yield at 420 nm amounted to 12.5%. H_2 evolved at a rate of 1.5 L h^{-1} m^{-2} under irradiation with a solar simulator (AM 1.5). Diffuse reflection and photoluminescence spectra of the solid solutions shifted monotonically to a long wavelength side, as the ratio of $CuInS_2$ to ZnS increased in the solid solutions. The photocatalytic H_2 evolution depended on the composition as well as the photophysical properties. DFT calculations suggested that the visible-light response should be derived from the contribution of Cu 3d and S 3p orbitals to the valence band and that of In 5s5p and Zn 4s4p orbitals to the conduction band, respectively. The contribution of these orbitals to the energy bands affected the photophysical and photocatalytic properties.

1. Introduction

The development of visible-light-driven photocatalysts for hydrogen evolution is a critical issue. The authors have previously succeeded in the development of visible-light-driven photocatalysts by doping of transition metal ions, such as Ni^{2+}, Cu^{2+}, and Pb^{2+}, into ZnS, which is a highly active photocatalyst for hydrogen evolution even without Pt cocatalysts under ultraviolet-light irradiation.[1−3] Especially, Ni- and Cu-doped ZnS photocatalysts showed high activities for the hydrogen evolution without any cocatalysts, and their apparent quantum yields were 1.3% and 3.7% at 420 nm, respectively. From the viewpoint of a different strategy from the doping, we also reported the $(AgIn)_xZn_{2(1-x)}S_2$ solid solution photocatalysts of which energy structures were able to be controlled by making a solid solution between a ZnS photocatalyst with a wide band gap and $AgInS_2$ with a narrow band gap. The photocatalytic activities and photophysical properties depended on the composition. Pt (3 wt %)-loaded $(AgIn)_{0.22}Zn_{1.56}S_2$ ($\sim AgInZn_7S_9$) with a 2.3-eV band gap showed the highest activity for H_2 evolution, and the apparent quantum yield at 420 nm amounted to 20%.[4] The visible-light response of the solid solution is due to the contributions of Ag and In to the valence and conduction bands, respectively. These results indicate that making a solid solution will be a leading strategy for development of new photocatalyst materials with visible-light response.

The ternary semiconductors of the I−III−VI_2 group (I = Cu, Ag; III = Al, Ga, In; VI_2 = S, Se, Te) with a chalcopyrite structure have attracted attention as new functional materials, especially in the field of solar cells. $CuInS_2$, $CuInSe_2$, and $Cu(In,Ga)Se_2$ including monovalent copper ions have intensively been investigated for a practical use in low-cost solar cell films instead of silicon and show high energy conversion efficiencies.[5−8] A number of solid solutions between chalcopyrite-type semiconductors have been reported.[8−10] The chalcopyrite structure is composed of tetrahedral units in which four anions coordinate to a cation. The unit cell of the chalcopyrite type can approximately be regarded as two unit cells of a zinc-blende type piled along the *c* axis. But, solid solutions between a chalcopyrite-type semiconductor and ZnS with a similar structure to chalcopyrite have been less-reported. Therefore, we have been interested in the photophysical and photocatalytic properties of their solid solutions.

It has been reported from some calculation techniques that the upper parts of valence bands of the I−III−VI_2 group (I = Cu, Ag; III = Al, Ga, In; VI = S, Se, Te) are composed of a d-state of Ag or Cu mixed with a p-state of S.[11,12] It has also been reported that the valence band level of $CuInS_2$ was more negative than those of ZnS and CdS.[13] A Cu 3d orbital in a Cu_2O semiconductor photoelectrode also contributes to the valence band formation.[14−16] Therefore, the monovalent copper cation is attractive as the component contributing to a visible-light response of solid solutions as well as the monovalent silver cation.

These facts have motivated us to be interested in the investigation of $(CuIn)_xZn_{2(1-x)}S_2$ solid solutions between ZnS and $CuInS_2$ as a new visible-light-driven photocatalyst in which Cu 3d orbitals contribute to the valence band formation. In the present paper, we prepared the series of ZnS−$CuInS_2$ solid solutions from Cu−In−Zn sulfide precursors obtained by coprecipitation using a H_2S gas as had been studied for the ZnS−$AgInS_2$ solid solution photocatalysts. The relationship

* Author to whom correspondence should be addressed. Fax: +81-33235-2214. E-mail: a-kudo@rs.kagu.tus.ac.jp.
[†] Tokyo University of Science.
[‡] Kurashiki University of Science and the Arts.
[§] Japan Science and Technology Agency.

10.1021/jp044722e CCC: $30.25
Published on Web 03/19/2005

among photophysical properties, photocatalytic activities, and band structures of the solid solutions was systematically studied. The comparison of the $(CuIn)_xZn_{2(1-x)}S_2$ solid solutions with the previously reported $(AgIn)_xZn_{2(1-x)}S_2$ solid solution photocatalysts was also discussed.

2. Experimental Section

2.1. Preparation and Characterization of Photocatalysts. A grayish precipitate of a Cu−In−Zn sulfide precursor was prepared by the following process. The mixed aqueous solution of $In(NO_3)_3 \cdot 3.6H_2O$ (Kojundo Chemical; 99.99%) and $Zn(NO_3)_2 \cdot 6H_2O$ (Wako Pure Chemicals; 99.0%) was bubbled with a N_2 gas, and then CuCl (Wako Pure Chemicals; 99.9%) was added into the solution. Each chemical was used in a stoichiometric molar ratio or with an excess amount of indium. Then, the precipitate of the Cu−In−Zn sulfide was produced by bubbling with a H_2S gas through the aqueous solution under vigorous stirring. The precipitate was washed with pure water and dried in air. The obtained powder was heat-treated at 1123 K for 5 h in an evacuated quartz ampule tube. The phases of the product were confirmed by X-ray diffraction (XRD; Rigaku; MiniFlex). Surface areas were determined by Brunauer−Emmett−Teller (BET) measurement (Coulter; SA3100). Diffuse reflection spectra were obtained using a UV−vis−near-IR spectrometer (Jasco; Ubest U-570) and were converted from reflection to absorbance by the Kubelka−Munk method. Photoluminescence spectra were measured in vacuo at 80 K using a spectrofluorometer (Spex; FluoroMax, photomultiplier tube R928P). Photocatalyst powders were observed by scanning electron microscopy (SEM; Hitachi; S-5000).

2.2. Photocatalytic Reactions. Photocatalytic reactions were conducted in a gas-closed-circulation system. The photocatalyst powder (0.3 g) was dispersed by a magnetic stirrer in an aqueous solution (300 mL) containing K_2SO_3 and/or Na_2S as electron donors in a side-window Pyrex reaction cell. The photocatalysts were irradiated with visible light ($\lambda \geq 420$ nm) through a cutoff filter (HOYA; L42) from a 300 W Xe lamp (ILC technology; Cermax LX-300). A solar simulator (Yamashita Denso; YSS-80QA) was also used in the test of the photocatalytic reaction under a simulated sunlight irradiation (AM 1.5). In this case, the amount of H_2 gas evolved was determined by a volumetric measurement. Pt and Ru cocatalysts were loaded by an in situ photodeposition method. An aqueous solution containing an appropriate amount of $H_2PtCl_6 \cdot 6H_2O$ (Tanaka Kikinzoku; 37.55% as Pt) or $RuCl_3 \cdot nH_2O$ (Wako; 99.9%) was mixed in the reactant solution. The amount of H_2 evolved was determined using inline gas chromatography (Shimadzu; GC-8A, MS-5A column, thermal conductivity detector, Ar carrier). The apparent quantum yields defined by the following equation were measured using filters combined with band-pass (Kenko) and cutoff (HOYA) filters, and a photodiode (Ophira; PD300-UV of a head and NOVA of a power monitor).

$$\mathrm{AQY}(\%) = \frac{\text{number of reacted electrons}}{\text{number of incident photons}} \times 100 = \frac{\text{number of evolved } H_2 \text{ molecules} \times 2}{\text{number of incident photons}} \times 100$$

2.3. Band Structure Calculation. The plane-wave-based density functional theory (DFT) calculation was carried out for ZnS with zinc-blende structure and $CuInS_2$ with chalcopyrite structure by employing the CASTEP program to obtain further information about the energy structure of the $(CuIn)_xZn_{2(1-x)}S_2$ solid solutions.[17] The core electrons were replaced with a norm-conserving pseudo-potential, and the valence electronic configurations for Zn, Cu, In, and S are $3d^{10}4s^2$, $3d^{10}4s^1$, $4d^{10}5s^25p^1$, and $3s^23p^4$, respectively. The kinetic energy cutoffs were taken to be 250 and 260 eV for ZnS and $CuInS_2$, respectively. The calculations were carried out using the primitive unit cells of [ZnS] and $[CuInS_2]_2$, which had 9 and 36 occupied orbitals, respectively. The atomic coordinates of ZnS and $CuInS_2$ were obtained from Yeh et al.[18] and Brandt et al.,[19] respectively.

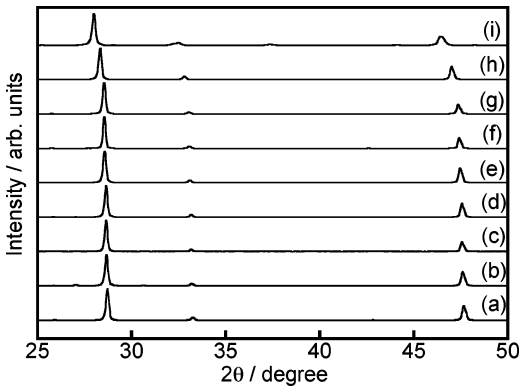

Figure 1. X-ray diffraction patterns of $(CuIn)_xZn_{2(1-x)}S_2$ solid solutions; the values of x are (a) 0, (b) 0.01, (c) 0.03, (d) 0.05, (e) 0.09, (f) 0.14, (g) 0.22, (h) 0.5, and (i) 1. Samples were heat-treated in a quartz ampule tube at 1123 K.

3. Results and Discussion

3.1. Crystal Structure. Figure 1 shows X-ray diffraction patterns of $(CuIn)_xZn_{2(1-x)}S_2$ solid solutions ($x = 0.5-0.01$). The solid solutions possessed a zinc-blende structure, but some of them contained a negligible amount of a wurtzite phase. The diffraction peaks shifted to the low-angle side of $CuInS_2$ as the value of x increased. The successive shift of the XRD pattern indicated that the crystals obtained were not mixtures of ZnS and $CuInS_2$ phases but rather the $(CuIn)_xZn_{2(1-x)}S_2$ solid solutions. The shift was reasonable because the ion radius of In^{3+} (0.76 Å) was larger than that of Zn^{2+} (0.74 Å) while Cu^+ (0.74 Å) had the almost same ion radius as Zn^{2+}.[20]

Figure 2 shows SEM images of a $(CuIn)_{0.03}Zn_{1.94}S_2$ solid solution. Well-crystallized particles with particle sizes of several micrometers were observed as shown in Figure 2a. The particles grown with a hexagonal plane were obtained around $x = 0.03$ in the compositions. The shape was specific for the solid solutions, whereas the shapes of ZnS and $CuInS_2$ particles prepared by similar methods to the solid solution were irregular. Figure 2b shows the Pt (3 wt %)-loaded $(CuIn)_{0.03}Zn_{1.94}S_2$ powders. Most of the Pt particles were selectively photodeposited on the hexagonal plane. Ohno et al. have reported that, in the case of the well-known TiO_2 photocatalyst, different crystal faces assist the separation of photogenerated electrons and holes and provide selective oxidation or reduction reaction sites.[21] Therefore, it was suggested that the particles of the solid solution had a specific reaction selectivity and the hexagonal planes mainly act as a reduction site.

3.2. Photophysical Properties. Figure 3 shows diffuse reflection spectra of $(CuIn)_xZn_{2(1-x)}S_2$ solid solutions ($x = 0.01-0.5$). The solid solutions with $x = 0.03-0.5$ had intense absorption bands with steep edges in a visible-light region. This shape indicated that the visible-light absorption was due to a band gap transition, not due to the transition from impurity levels to the conduction band of ZnS as observed for the metal-ion-doped ZnS photocatalysts.[1-3] The absorption edges of $(CuIn)_xZn_{2(1-x)}S_2$ were in a position between those of ZnS and $CuInS_2$,

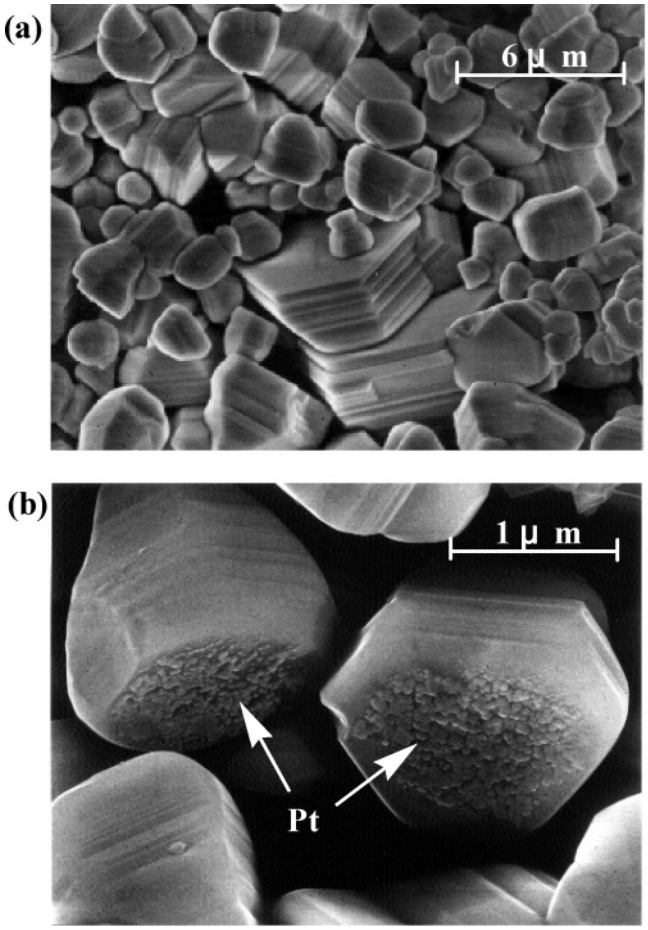

Figure 2. Scanning electron microscope images of the $(CuIn)_{0.03}Zn_{1.94}S_2$ solid solution heat-treated in a quartz ampule tube at 1123 K; (a) nonloaded and (b) Pt (3 wt %)-loaded in 0.5 M K_2SO_3 solution.

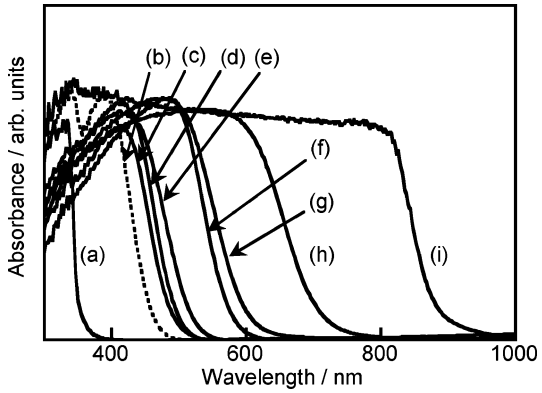

Figure 3. Diffuse reflection spectra of $(CuIn)_xZn_{2(1-x)}S_2$ solid solutions; the values of x are (a) 0, (b) 0.01, (c) 0.03, (d) 0.05, (e) 0.09, (f) 0.14, (g) 0.22, (h) 0.5, and (i) 1. Samples were heat-treated in a quartz ampule tube at 1123 K.

and the band gap became narrow monotonically as the value of x was increased. The band gaps of the solid solutions were estimated to be 1.75−2.67 eV ($x = 0.01-0.5$) from the onsets of absorption edges. The absorption spectrum of $x = 0.01$ was split into two peaks at 337 and 390 nm, being different from other compositions. The split of the absorption band suggested that the transition was not the band gap transition but the transition from discrete donor levels to the conduction band.

The $(CuIn)_xZn_{2(1-x)}S_2$ solid solutions ($x = 0.05-0.22$) showed broad photoluminescence spectra in the visible-light region longer than their absorption edges at 80 K as shown in Figure 4A. The onsets of the excitation spectra were almost the same

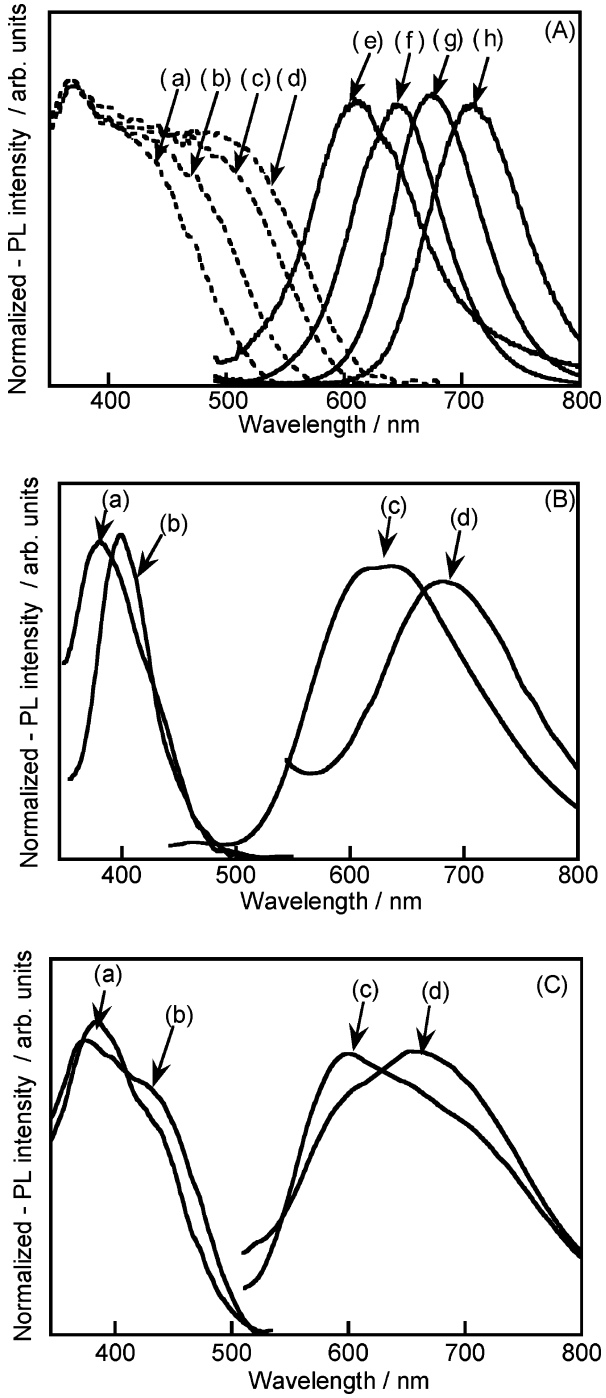

Figure 4. (A) Photoluminescence spectra of $(CuIn)_xZn_{2(1-x)}S_2$ solid solutions at 80 K. Excitation spectra: (a) $x = 0.05$ monitored at 630 nm; (b) $x = 0.09$ monitored at 645 nm; (c) $x = 0.14$ monitored at 672 nm; (d) $x = 0.22$ monitored at 710 nm. Emission spectra: (e) $x = 0.05$; (f) $x = 0.09$; (g) $x = 0.14$; (h) $x = 0.22$, excited at 467 nm, respectively. (B) Photoluminescence spectra of $(CuIn)_{0.01}Zn_{1.98}S_2$ solid solutions at 80 K. Excitation spectra: (a) monitored at 680 nm; (b) monitored at 630 nm. Emission spectra: (c) excited at 380 nm; (d) excited at 467 nm. (C) Photoluminescence spectra of $(CuIn)_{0.03}Zn_{1.94}S_2$ solid solutions at 80 K. Excitation spectra: (a) monitored at 598 nm; (b) monitored at 700 nm. Emission spectra: (c) excited at 380 nm; (d) excited at 467 nm.

positions as those of diffuse reflection spectra, indicating that these emissions were derived from band gap excitation. The photoluminescence spectra shifted successively with a change in the composition as well as the diffuse reflection spectra. The photophysical properties of absorption and photoluminescence spectra revealed that the energy structures of the $(CuIn)_xZn_{2(1-x)}S_2$

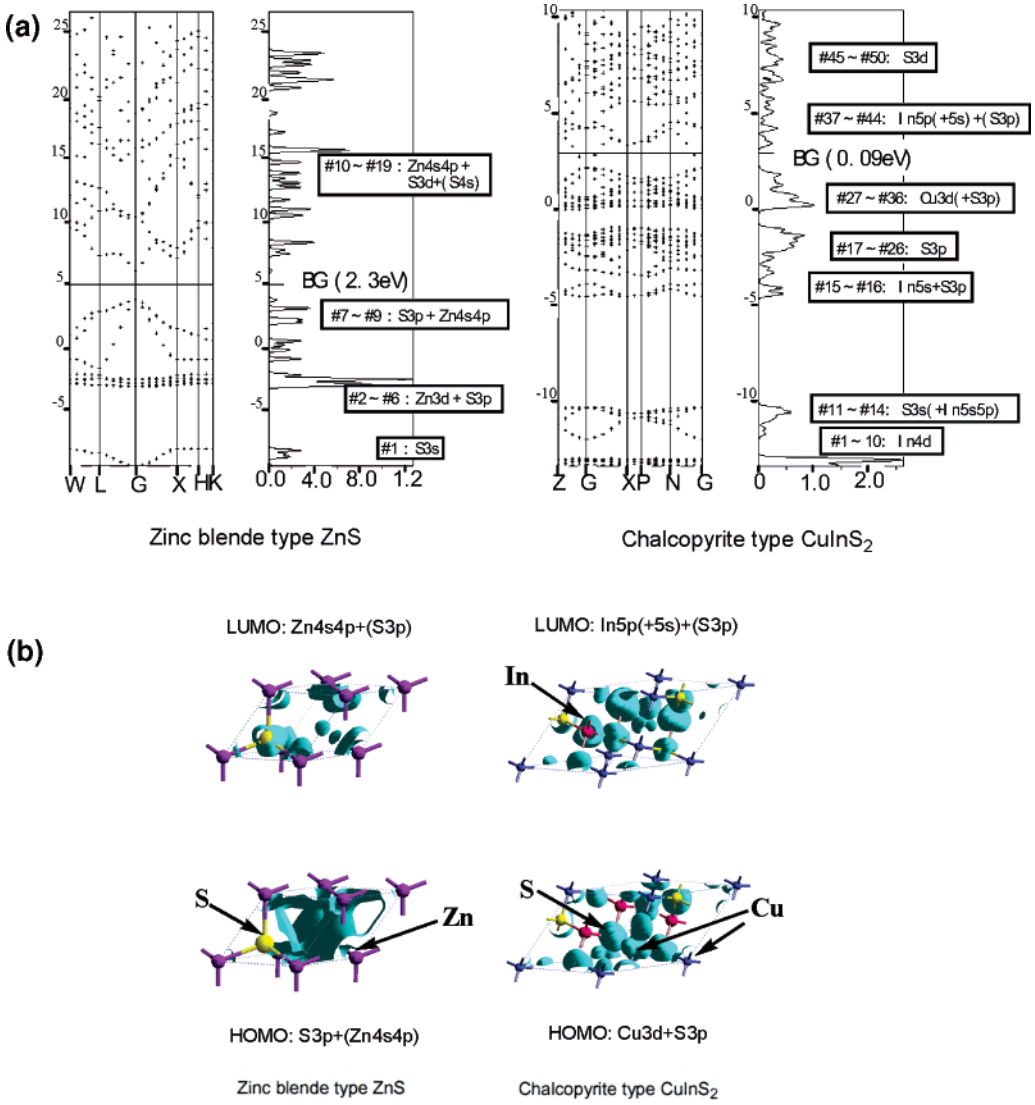

Figure 5. (a) Band structures and densities of states for ZnS and $CuInS_2$ calculated by the density functional method. (b) Density contour maps for the LUMOs and HOMOs of ZnS and $CuInS_2$.

solid solutions were dependent on the value of x. However, the solid solutions of $x = 0.01$ and 0.03 showed broad emission bands with some peaks in the 600−700-nm range as shown in Figures 4, parts B and C, being different from other compositions that showed the almost single emission spectrum. Moreover, the peak positions of $x = 0.01$ and 0.03 were different from those expected from the successive shift of $x = 0.05-0.22$. These results indicated that not bands but discrete impurity levels of Cu^+ and In^{3+} were formed in a forbidden band as the value of x became small. The diffuse reflection spectra of $x = 0.01$ with the spilt absorption bands also suggested the formation of discrete levels (Figure 3). The emission intensities of $(CuIn)_x$-$Zn_{2(1-x)}S_2$ solid solutions were dependent upon the composition ($x = 0.03-0.22$) at 80 K. The most intensive luminescence was observed at $x = 0.14$. The intensities of the solid solutions were remarkably decreased as the value of x became smaller than 0.14. This result revealed that the absorption bands, of which Cu and In contributed to the formation, became discrete and acted as the trapping centers of photogenerated electrons and holes when a value of x became much small ($x < 0.14$).

3.3. Band Structures. Figure 5a shows the band structures and the densities of state (DOS) of ZnS and $CuInS_2$. The density contour maps for the lowest unoccupied molecular orbitals (LUMOs) and highest occupied molecular orbitals (HOMOs) of ZnS and $CuInS_2$ are shown in Figure 5b. Most orbitals of ZnS were made up of hybrid orbitals of Zn and S due to the covalency except for the orbital of the lowest-energy side (#1) as shown in Figure 5a. Therefore, the valence band maximum (HOMO, #9) and conduction band minimum (LUMO, 10) of ZnS were also made up of S 3p and Zn 4s4p hybrid orbitals as shown in Figure 5b. The occupied bands of $CuInS_2$ were classified into five bands. The lower-energy side in the occupied bands consisted of In 4d (#1−10) and S 3s (+ In 5s5p) (#11−14) orbitals, respectively. The middle part of the occupied bands consisted of In 5s + S 3p hybrid orbitals (#15−16) and S 3p orbitals (#17−26), respectively. The higher-energy side (i.e., a valence band) was composed of Cu 3d (+S 3p) hybrid orbitals (#27−36). The valence band maximum (HOMO, #36) was made up of Cu 3d orbital hybridized with S 3p as shown in Figure 5b. The conduction band minimum (LUMO, #37) and the successive orbitals constituting the lower-energy side of conduction band (#37−44) were composed of In 5p(5s) orbitals hybridized by S 3p orbitals. The high-energy side (#45−50) consisted of solely S 3d orbitals. The contribution of S 3p orbitals to the conduction band indicated that the covalent band characteristic of $CuInS_2$ was as large as ZnS. The calculated band gap energies of ZnS and $CuInS_2$ were 2.3 and 0.09 eV, respectively. The order of the band gap energy of ZnS and

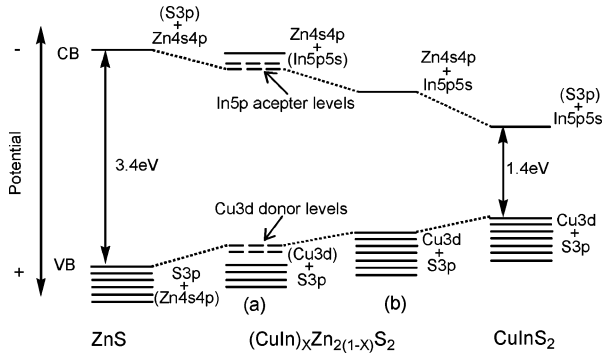

Figure 6. Band structures of $(CuIn)_xZn_{2(1-x)}S_2$ solid solutions, ZnS, and $CuInS_2$.

$CuInS_2$ was the same as that in the experimental values estimated from the diffuse reflection spectra, although the calculated band gap of $CuInS_2$ was extremely smaller than the experimental value. It was also reported from other calculation techniques that the upper part of a valence band of $CuInS_2$ was composed of a d-state of Cu mixed with a p-state of S.[11,12] These results were in good agreement with our results obtained by the plane-wave-based method.

The results of the photophysical properties and DFT calculations led us to the band structure of the $(CuIn)_xZn_{2(1-x)}S_2$ solid solution between ZnS and $CuInS_2$ as shown in Figure 6. Both S 3p and Cu 3d orbitals contributed to the makeup of a valence band in a $(CuIn)_xZn_{2(1-x)}S_2$ solid solution. The valence band maximum (HOMO) should also be composed of the hybrid orbitals of S 3p and Cu 3d as in the case of $CuInS_2$. In 5s5p orbitals mixed with Zn 4s4p contributed to formation of the conduction band. The conduction band minimum (LUMO) was also made up of the In 5s5p + Zn 4s4p hybrid orbital. The positions of the HOMO and LUMO of the solid solution should be located between those of ZnS and $CuInS_2$, and the potentials of the valence and conduction band levels were able to be controlled successively by a change in the ratio of $CuInS_2$ to ZnS. Valence and conduction bands consisting of Cu and In were formed when the value of x was large as shown in Figure 6b. On the contrary, the discrete levels composed of Cu and In were formed in a forbidden band as the concentration of their components became low as shown in Figure 6a. The proposed band structure of the solid solution was reasonable judging from the diffuse reflection and photoluminescence spectra. These observations show that the $(CuIn)_xZn_{2(1-x)}S_2$ solid solutions are promising materials with controllable energy structure and are expected to be new visible-light-driven photocatalysts if the conduction band level is high enough to reduce H_2O to form H_2.

3.4. Photocatalytic Activities of $(CuIn)_xZn_{2(1-x)}S_2$ Solid Solutions. Table 1 shows the effect of composition on the photocatalytic activities of nonloaded and Pt (0.5 wt %)-loaded $(CuIn)_xZn_{2(1-x)}S_2$ solid solutions for H_2 evolution from an aqueous solution containing SO_3^{2-} as a sacrificial reagent under visible-light irradiation. The photocatalytic activity of the solid solution depended upon the composition. $CuInS_2$ with a narrow band gap and ZnS photocatalyst with a wide band gap hardly possessed activities for H_2 evolution under visible-light irradiation ($\lambda \geq 420$ nm) even in the presence of Pt cocatalysts. The small photocatalytic activity of ZnS itself might be due to little visible-light absorption by some impurity levels. In contrast, the $(CuIn)_xZn_{2(1-x)}S_2$ solid solutions showed high photocatalytic activities for H_2 evolution under visible-light irradiation when Pt cocatalysts that worked as active sites for H_2 evolution were loaded on the photocatalysts. The dependency of the H_2 evolution reaction upon the composition would be mainly due to the change in the band structure. The activities of nonloaded and Pt-loaded $(CuIn)_xZn_{2(1-x)}S_2$ solid solutions were increased as the value of x became small. It indicated that the conduction band that had a high enough potential to reduce H_2O to H_2 was formed as the ratio of ZnS to $CuInS_2$ was increased. Especially, the activities of nonloaded photocatalysts were monotonically increased as the value of x became small. The result suggested that the conduction band level was a main factor to affect the photocatalytic activity in the case of a nonloaded photocatalyst. However, Pt-loaded photocatalysts showed the highest activities around the compositions $x = 0.05-0.09$. The quantum yield of the Pt (0.5 wt %)-loaded $(CuIn)_{0.09}Zn_{1.82}S_2$ photocatalyst at 420 nm amounted to 12.5%. Even under the simulated sunlight irradiation (AM 1.5), the photocatalyst showed that H_2 gas evolved at a rate of 1.5 L h^{-1} m^{-2}; it was comparatively high even in the presence of sacrificial reagents, except for the Pt-loaded CdS photocatalyst (QY $\approx$ 37%)[22,23] that includes harmful cadmium. The activities of Pt-loaded photocatalysts were decreased when x became lower than 0.09. These observations indicated that the photocatalytic activities depended upon not only the conduction band level but also the other factors. One of the reasons for the decrease in the activity is that the absorption bands consisting of Cu and In became discrete as the value of x was much small, as mentioned in the band structure section. It would result in the decrease in the mobility of photogenerated carriers, which is an important factor affecting the photocatalytic activity. The discrete levels also act as the recombination centers of electrons and holes. Another possible inactivation factor is that the number of available photons decreased with the extension of a band gap. However, the absorption spectra of $x = 0.03-0.09$ were not shifted significantly as shown in Figure 3, indicating that the activity was less affected by the number of available photons.

TABLE 1: Dependence of Photocatalytic Activities for H_2 Evolution From an Aqueous K_2SO_3 Solution over $(CuIn)_xZn_{2(1-x)}S_2$ Solid Solutions upon the Value of x[a]

		rate of H_2 evolution (μmol h^{-1})	
value of x	band gap (eV)	nonloaded	Pt-loaded
0	3.50	10	11
0.01	2.67	30	308
0.03	2.53	14	251
0.05	2.48	9	556
0.09	2.35	7	684
0.14	2.15	5	224
0.22	2.07	2	35
0.50	1.75	0.1	2
1	1.40	0.05	0.9

[a] Catalysts, 0.3 g; heat-treated in a quartz ampule tube at 1123 K; reactant solution, 300 mL (0.5 M K_2SO_3); light source, 300 W Xe lamp with a cutoff filter ($\lambda \geq 420$ nm).

Figure 7 shows the H_2 evolution under visible-light irradiation from aqueous solutions containing sacrificial reagents over $(CuIn)_{0.09}Zn_{1.82}S_2$ solid solution photocatalyst that showed the highest activity. An aqueous solution containing K_2SO_3 and the mixed solution containing both K_2SO_3 and Na_2S as electron donors were employed. Ru was also used as a cocatalyst instead of Pt. The activities of Pt-loaded photocatalysts were considerably high under the two different reactant solutions although slight deactivations were observed during the photocatalytic reactions (Figure 7, parts a and b). On the contrary, Ru-loaded photocatalysts showed different reactivity from Pt-loaded photocatalysts. Although the hydrogen evolution was very low under the K_2SO_3 solution, it showed significantly high activity under the mixed solution containing both K_2SO_3 and Na_2S (1227 μmol

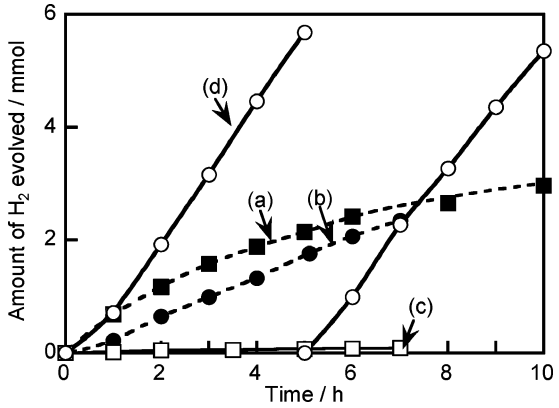

Figure 7. Photocatalytic H_2 evolution under visible-light irradiation over the $(CuIn)_{0.09}Zn_{1.56}S_2$ solid solution heat-treated in a quartz ampule tube at 1123 K. Pt (0.5 wt %)-loaded photocatalyst in (a) K_2SO_3 (0.5 M), (b) K_2SO_3 (0.25 M)−Na_2S (0.35 M) aqueous solution. Ru (0.5 wt %)-loaded photocatalyst in (c) K_2SO_3 (0.5 M), (d) K_2SO_3 (0.25 M)−Na_2S (0.35 M) aqueous solution. The reaction solution was replaced after 5 h. Catalyst, 0.3 g; light source, 300 W Xe lamp with a cutoff filter ($\lambda \geq 420$ nm); reaction cell, side-window Pyrex cell.

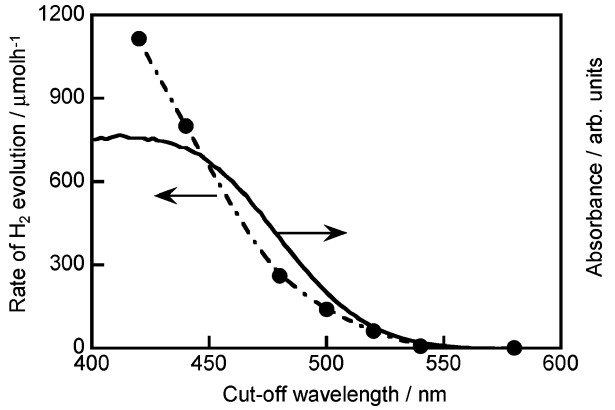

Figure 8. Dependence of H_2 evolution from an aqueous K_2SO_3 (0.25 mol L^{-1})−Na_2S (0.35 mol L^{-1}) solution (300 mL) over the $(CuIn)_{0.09}Zn_{1.82}S_2$ solid solution upon cutoff wavelengths of filters. Catalyst, 0.3 g; light source, 300 W Xe lamp with cutoff filters; reaction cell, side-window Pyrex cell.

h^{-1} at the initial stage of the reaction). The activity of Ru-loaded photocatalyst was comparatively stable over 10 h of reaction time if the reaction solution was replaced periodically with fresh solutions, as shown in Figure 7d. Remarkable changes in the XRD patterns were not observed before and after the reaction, indicating that the photocatalyst was stable under the reaction condition.

Figure 8 shows the dependence of hydrogen evolution from an aqueous K_2SO_3 and Na_2S solution over Ru (0.5 wt %)-loaded $(CuIn)_{0.09}Zn_{1.82}S_2$ photocatalyst upon a cutoff wavelength using cutoff filters. The onset of the action spectrum agreed well with that of the diffuse reflection spectrum. It was revealed that the visible-light response of the photocatalyst is due to the band gap transition between the valence band and the conduction band controlled by making a solid solution.

3.5. Comparison of Photophysical and Photocatalytic Properties of $(CuIn)_xZn_{2(1-x)}S_2$ with Those of $(AgIn)_xZn_{2(1-x)}S_2$. It was found that the zinc-blende-type $(CuIn)_xZn_{2(1-x)}S_2$, for which the energy structure (band position) was controllable by changing the composition, was an active photocatalyst for H_2 evolution under visible-light irradiation as well as the wurtzite-type $(AgIn)_xZn_{2(1-x)}S_2$ solid solution that the authors have previously reported.[4] Figure 9 shows a comparison of the diffuse reflection spectra of Cu systems with those of Ag systems. The

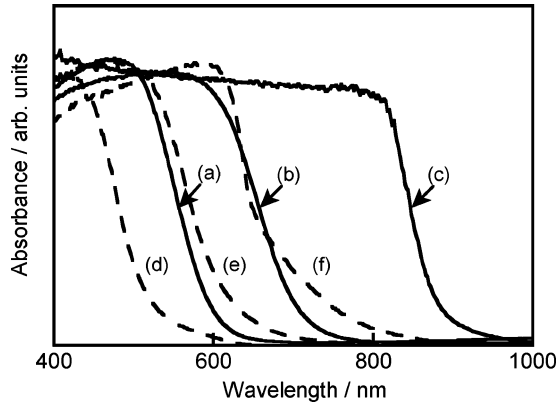

Figure 9. Diffuse reflection spectra of $(MIn)_xZn_{2(1-x)}S_2$ solid solutions and $MInS_2$. Cu systems (M = Cu): (a) $x = 0.22$, (b) $x = 0.5$, and (c) $CuInS_2$. Ag systems (M = Ag): (d) $x = 0.22$, (e) $x = 0.5$, and (f) $AgInS_2$.

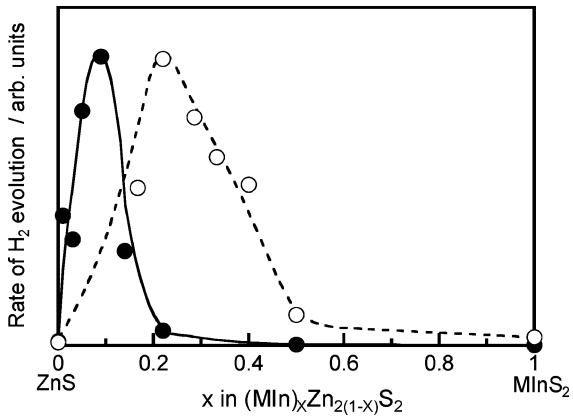

Figure 10. Dependence of photocatalytic H_2 evolution from an aqueous K_2SO_3 (0.5 mol L^{-1}) under visible-light irradiation over the Pt-loaded $(MIn)_xZn_{2(1-x)}S_2$ solid solutions: (●) M = Cu, (○) M = Ag. Catalyst, 0.3 g; light source, 300 W Xe lamp with a cutoff filter ($\lambda \geq 420$ nm); reaction cell, side-window Pyrex cell.

absorption bands of $(CuIn)_xZn_{2(1-x)}S_2$ ($x = 0.22$ and 0.5) solid solutions were in a position at a longer wavelength side than those of $(AgIn)_xZn_{2(1-x)}S_2$ ($x = 0.22$ and 0.5), like the relationship between $CuInS_2$ and $AgInS_2$. Because the valence band level consisting of Cu 3d orbitals is higher than that of Ag 4d orbitals, the band gaps of Cu systems are narrower than those of Ag systems. Crystal structure is also another possible factor to affect a band gap. In some sulfides such as ZnS, CdS, and $AgInS_2$, which have a similar crystal structure, band gaps of the low-temperature phase (zinc-blende- or chalcopyrite-type) are around 0.1 eV smaller than that of the high-temperature phase (wurtzite-type).[24,25] Therefore, the crystal structure depending upon the component of Cu and Ag may also affect the band gap in the series of the solid solutions. The investigation of a new $(CuIn)_xZn_{2(1-x)}S_2$ solid solution photocatalyst that absorbs long wavelength visible-light is meaningful for the usage of solar light.

Figure 10 shows the dependence of photocatalytic activities for H_2 evolution from an aqueous K_2SO_3 solution over $(MIn)_xZn_{2(1-x)}S_2$ (M = Cu, Ag) solid solutions upon the value of x. The rates of H_2 evolution of $(CuIn)_xZn_{2(1-x)}S_2$ and $(AgIn)_xZn_{2(1-x)}S_2$ were normalized because the preparation and experimental conditions were different in each case. The photocatalytic activities of the two types of solid solutions depended on their compositions. However, the compositions that showed the highest activities (i.e., Cu system, $x = 0.09$; Ag system, $x = 0.22$) and the compositions at which H_2 evolution

was observed (i.e., Cu system, $x = 0.22$; Ag system, $x = 0.50$) were different for each system. This is due to the fact that the wurtzite-type $(AgIn)_xZn_{2(1-x)}S_2$ with a wider band gap would possess a conduction band level higher than that of the zinc-blende-type $(CuIn)_xZn_{2(1-x)}S_2$ with a narrower band gap even at the same compositions.

Conclusions

It was found that $(CuIn)_xZn_{2(1-x)}S_2$ was an active solid solution photocatalyst for H_2 evolution under visible-light irradiation as well as the $(AgIn)_xZn_{2(1-x)}S_2$ photocatalysts that the authors have previously reported. The series of solid solutions had energy bands that were controllable with the concentration of Cu, Ag, and In components contributing to band formations. The photophysical and photocatalytic properties were dependent on the energy structure with the changing composition of the solid solutions. Pt (0.5 wt %)-loaded $(CuIn)_{0.09}Zn_{1.82}S_2$ with a 2.3-eV band gap showed the highest activity for H_2 evolution, and the apparent quantum yield at 420 nm amounted to 12.5%. The stability of the activity was much improved by the deposition of a Ru cocatalyst. $(CuIn)_xZn_{2(1-x)}S_2$ had absorption bands at a longer wavelength side than those of $(AgIn)_xZn_{2(1-x)}S_2$ since the valence bands composed of the Cu 3d and S 3p hybrid orbitals were formed at a more negative level than those of Ag 4d and S 3p hybrid orbitals and the difference of crystal structures also affected the band structure. The present results indicate that a monovalent copper ion is a promising element to construct a stable valence band contributing to a visible-light response.

Acknowledgment. This work was supported by the Core Research for Evolutional Science and Technology (CREST), a Grant-in-Aid for the Priority Area Research (No. 417) from the Ministry of Education, Culture, Science, and Technology, and the Tokyo Ohka Foundation for the Promotion of Science and Technology.

References and Notes

(1) Kudo, A.; Sekizawa, M. *Chem. Commun.* **2000**, 1371.
(2) Kudo, A.; Sekizawa, M. *Catal. Lett.* **1999**, *58*, 241.
(3) Tsuji, I.; Kudo, A. *J. Photochem. Photobiol., A* **2003**, *156*, 249.
(4) Tsuji, I.; Kato, H.; Kobayashi, H.; Kudo, A. *J. Am. Chem. Soc.* **2004**, *126*, 13406.
(5) Klaer, J.; Bruns, J.; Henninger, R.; Siemer, K.; Klenk, R.; Ellmer, K.; Braunig, D. *Semicond. Sci. Technol.* **1998**, *13*, 1456.
(6) Lokhande, C. D.; Barkschat, A.; Tributsch, H. *Sol. Energy Mater. Sol. Cells* **2000**, *79*, 293.
(7) Abushama, J. A. M.; Johnston, S.; Moriarty, T.; Teeter, G.; Ramanathan, K.; Noufi, R. *Prog. Photovol. Res. Appl.* **2004**, *12*, 39.
(8) Kannan, R.; A, C. M.; L, P. C.; Sally, A.; S, H. F.; James, K.; David, Y.; Manuel, R.; Wyatt, M.; Rommel, N.; James, W.; Anna, D. *Prog. Photovol. Res. Appl.* **2003**, *11*, 225.
(9) Chichibu, S.; Harada, Y.; Sugiyama, M.; Nakanishi, H. *J. Phys. Chem. Solids* **2003**, *64*, 1481.
(10) Bodnar, I. V.; Korzun, B. V.; Yashukevich, L. V. *Russ. J. Inorg. Chem.* **1998**, *43*, 771.
(11) Lavrentiev, A. A.; Gabrelian, B. V.; Nikiforov, I. Y. *J. Struct. Chem.* **2000**, *41*, 418.
(12) Rashkeev, S. N.; Lambrecht, W. R. L. *Phys. Rev. B* **2001**, *63*, 165212.
(13) Hunger, R.; Pettenkofer, C.; Scheer, R. *Surf. Sci.* **2001**, *477*, 76.
(14) Fernando, C. A. N.; Bandara, T. M. W. J.; Wethasingha, S. K. *Sol. Energy Mater. Sol. Cells* **2001**, *70*, 121.
(15) Brahms, S.; Nikitine, S. *Phys. Lett.* **1966**, *22*, 31.
(16) Ruiz, E.; Alvarez, S. *Phys. Rev. B* **1997**, *56*, 71789.
(17) Payne, M. C.; Teter, M. P.; Allan, D. C.; Arias, T. A.; Joannopoulos, J. D. *Rev. Mod. Phys.* **1992**, *64*, 1045.
(18) Yeh, C.; Lu, Z. W.; Froyen, S.; Zunger, A. *Phys. Rev. B* **1992**, *46*, 10086.
(19) Brandt, G.; Raeuber, A.; Schneider, J. *Solid State Commun.* **1973**, *12*, 481.
(20) Shannon, R. *Acta Crystallogr., Sect. A* **1976**, *32*, 751.
(21) Ohno, T.; Sarukawa, K.; Matsumura, M. *New J. Chem.* **2002**, *26*, 1167.
(22) Mau, A. W.-H.; Huang, C. B.; Kakuta, N.; Bard, A. J. *J. Am. Chem. Soc.* **1984**, *106*, 6537.
(23) Reber, J. F.; Rusek, M. *J. Phys. Chem.* **1986**, *90*, 824.
(24) Shionoya, S.; Yen, W. M. *Phosphor Handbook*; CRC: New York, 1999.
(25) Shay, J. L.; Tell, B.; Schiavone, L. M. *Phys. Rev. B* **1974**, *9*, 1719.